Biol. Cybern. 52, 23–36 (1985)

Biological Cybernetics

Mathematical Analysis of the Stimulus for the Lateral Line Organ

El-S. Hassan

Arbeitsgruppe III (Biophysik), Institut für Zoologie, Johannes-Gutenberg-Universität, Saarstrasse 21, D-6500 Mainz, Federal Republic of Germany

Abstract. Behavioral studies have shown that a blind fish is capable of detecting and recognizing stationary objects in its surroundings. It is proposed that the displacement of water caused by the fish as it moves is the basis for this detection capability. Alterations in the displacement of water around the fish, caused by the obstacle, act as stimuli for the lateral line organ. The question of how these stimuli acting on the skin of the fish, image the environment and what information is thus made available to the fish is the concern of this paper. The stimuli for the lateral line organ are derived mathematically. Two cases are treated: that of a fish gliding past an obstacle and that of one approaching an obstacle.

1 Introduction

When a fish glides through water, a current field is set up around its body due to the displacement of water at its head and the suction at its tail. An obstacle in the vicinity of the fish will alter this current field as shown schematically in Fig. 1. The alterations in the water displacement on the skin of the fish will depend on the obstacle's size and shape, and on its distance from the fish. These alterations act as stimuli for the lateral line organ. If the fish were able to evaluate these stimuli, this would be a way for it to recognize objects in its surroundings.

On the basis of this hypothesis (v. Campenhausen et al., 1981), behavioral experiments have been carried out on the blind cave fish Anoptichthys jordani (Weissert and v. Campenhausen, 1981). The results of these experiments show that the fish is able to discriminate between stationary objects with respect to their shape. It should be noted here that the range for this discriminatory capability seems to be limited to a small distance away from the fish. The range within which a fish can detect a stationary object such as the aquarium wall is limited to a few centimeters (Dijkraaf, 1962). However, a fish can detect smaller objects, e.g., thin bars with diameters down to 2 mm, at a distance of few millimeters (v. Campenhausen et al., 1981).

The lateral line organ responds to the movement of the water relative to the fish's skin (Dijkraaf, 1934, 1967). The cupulae of the free neuromasts, which are arranged in certain patterns on the head and the body surface, are affected by a shear motion due to the water displacement and thus excite the hair cells which are connected with the cupulae by means of sensory cilia (Görner, 1961; Flock and Wersäll, 1962). By contrast, the cupulae of the neuromasts in the canal organ are situated in canals beneath the skin, which are in contact with the external medium via pores. When a pressure difference in the external medium arises between the outer openings of the pores, the fluid inside the canals is shifted. This subjects the cupulae between the pores to a shear motion and thus excites the hair cells (Dijkraaf, 1952; Kuiper, 1967). Consequently, the water displacement and the pressure gradients on the body surface of the fish constitute the stimuli for the lateral line system with the aid of which the fish, according to the above hypothesis, can scan its surroundings. This gives rise to the questions of how these stimuli acting on the skin of a moving fish image the environment and what information is thus made

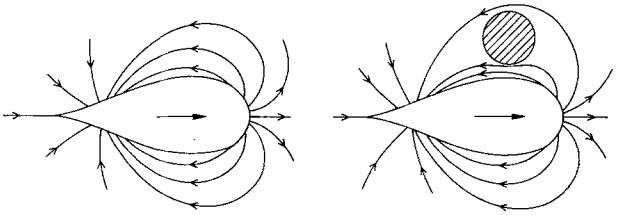

Fig. 1. Schematic diagram of the current flow around a gliding fish. Left: in open water. Right: passing an obstacle

available to it. The aim of this paper is to investigate these questions by determining mathematically the spatial and temporal course of the stimuli on the skin of a fish gliding past or approaching an obstacle.

In this context it must be noted that the current field produced by a moving fish depends on the fish's shape. So it can be expected that the shape of the fish will also play a role in the detection mechanism. There is a great variety in the body shape of fishes, and this can be correlated with performance criteria (Webb, 1978, 1984). Consider a fish of disk-like shape with large flat sides. The current field produced by a moving fish of this shape can be approximated for the middle region along the fish's sides by a two-dimensional field. This is possible because the gradient of this field will be small in the dorso-ventral direction from the middle region due to the flatness of the fish's body. This assumption makes it possible to apply powerful methods used in hydrodynamics for the analysis of two-dimensional fields. In this context the following analysis will be carried out for obstacles with the shape of a cylindrical bar oriented parallel to the dorso-ventral axis of the fish and the results will be restricted to the middle region along the fish's side where the canal organ is located. For the field currents at any locus of the fish's surface and for fish of other shapes, a three-dimensional description is to be preferred. The present analysis is restricted to the two-dimensional case.

2 Methods

2.1 Presuppositions for the Computation

1. The current field around a fish gliding in open water can be simulated by a certain configuration of sources in the head region and sinks in the tail region. Equating the gliding fish's body with this configuration of singularities, whose current field functions are known, makes it possible to describe the current field around the fish mathematically.

2. A stationary object in the vicinity of a gliding fish will alter the fish's current field. In mathematical terms this alteration can be described as resulting from the influence of a configuration of singularities induced in the object by the moving fish. The substitute configuration for the object depends on its shape and size, and on its position relative to the fish and is determined by means of the method of images (cf. e.g., Curle and Davies, 1968).

3. When a stationary object is introduced into the current field of the gliding fish, care must be taken that the calculated current still runs parallel to the surface of the fish's body. To avoid theoretical currents crossing the surface of the fish, the substitute configuration of the object has to be imaged in the fish's body. This entails a new substitute configuration for the fish's body which in turn must be imaged in the object.

From this it can be seen that an interaction between real bodies and a current field can be described by an infinite series of singularity substitute configurations. The resulting current is then the vectorial summation of all component currents caused by the individual singularities in this series. The prerequisite is, of course, that the series converges. Fields of this type, which depend on the influence of two objects are called double periodic (cf. e.g., Betz, 1964). In a few cases a closed mathematical formula can be found for them, depending on the geometry of the bodies involved. If, as in our case, this is not possible an iteration procedure has to be applied until a certain exactitude has been achieved. This is the approach used in this paper.

4. The method of images has been developed in the two-dimensional case for the application to straight lines and circles. But so far no similar method is known for directly calculating the current for the fish shape (cf. Curle and Davies, 1968). In two-dimensional space, however, it is possible to transform a fish-like shape in a plane into a circle in another plane by a conformal mapping. In this other plane, the method of images can be applied to the circle so that, after retransformation into the original plane, the substitute configuration for the fish-like shape can be obtained. In two-dimensional space the situation corresponds to that of a gliding cylinder with a fish-shaped cross-section (dorsal view of a fish) with a stationary circular cylinder in its current field (as indicated in Fig. 1). In the following, the term "gliding cylinder" will be used for the fish and "stationary cylinder" for the obstacle.

5. Finally it is assumed that the temporal alteration of the current field does not occur too rapidly so that, for any instant in time, it can be assumed to be stationary and the current to be laminar. The current field can then be calculated for a series of instants in time, i.e., for a series of positions of the gliding cylinder relative to the stationary cylinder.

2.2 Description of the Individual Steps

The calculation was divided into a sequence of steps according to the above assumptions. Figure 2 shows this sequence diagrammatically. The details of the conformal transformation will be treated later, so for the moment, the reader is asked to pay attention to the fish-shaped figure and the solid line circle.

Step 1): The gliding cylinder (g. Cyl.) is replaced by a configuration of singularities (SC).

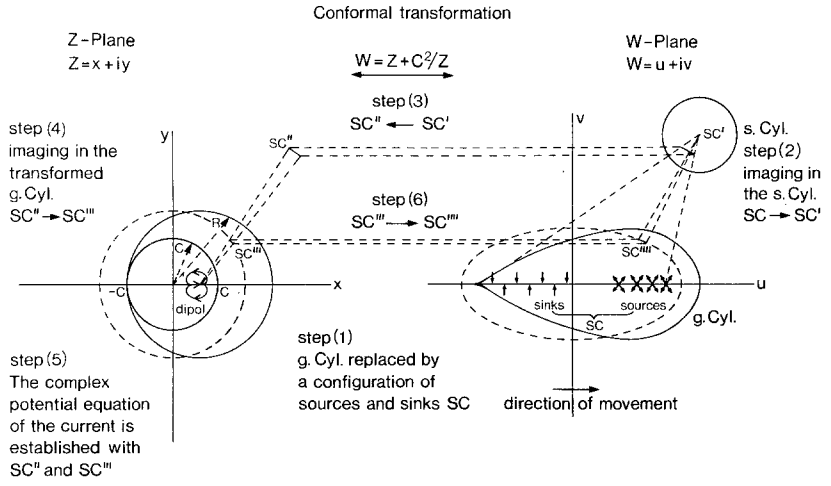

Fig. 2. Schematic diagram of the procedure for calculating the current velocity distribution on the surface of a cylinder gliding past a stationary cylinder; g. Cyl. = gliding cylinder; s. Cyl. = stationary cylinder

Step 2): The substitute configuration for the g. Cyl. is imaged in the stationary cylinder (s. Cyl.) generating a new configuration SC′ which replaces the s. Cyl. with respect to its influence on the current field.

Step 3): The imaging of SC′ in the g. Cyl. (required by presupposition 3. above) can only be performed after transformation of SC′ by means of a conformal mapping from its plane (W plane) into another plane (Z plane) where the cross-section shape of the g. Cyl. can be transformed into a circle. Step 3 is then the conformal mapping of SC′ into a corresponding configuration SC″ in the Z plane.

Step 4): The transformed configuration SC″ in the Z plane is imaged in the transformed circle of the g. Cyl. This generates a new configuration SC‴ which fulfills the requirement that the current must run parallel to the surface of the g. Cyl.

Step 5): The complex current field function is established with the substitute configurations SC″ and SC‴ which are then used to ascertain the values of the current velocities at the contour lines of the circle corresponding to the g. Cyl. Since the point of departure is the configuration SC″ substituted for the s. Cyl., the values ascertained for the current velocities represent exclusively the changes due to the presence of the s. Cyl. in the current field. The values obtained for the change in the current velocity in the Z plane then have to be multiplied by a transformation factor to obtain the corresponding values for the W plane.

Step 6): The newly generated configuration SC‴ must now be imaged in the s. Cyl. in accordance with presupposition 3. Since the s. Cyl. no longer has a circular cross-section in the Z plane, SC‴ must be retransformed to a corresponding configuration SC⁗ in the W plane. SC⁗ can then be imaged in the s. Cyl. in the W plane.

This brings the procedure back to Step 2 again. The whole procedure is then repeated from Step 2 onwards as many times as is necessary to obtain values for the current velocity change which are added together until the additionally gained values are so small they can be neglected. This is definitely the case if the distance between sources and sinks becomes so small that they neutralize each other.

2.3 Calculation of the Substitute Configuration for the Gliding Cylinder

This paper will deal with three cases with three different cross-section shapes for the gliding cylinder, viz., circle, ellipse and fish-shape (dorsal view of a fish). The cross-section of the stationary cylinder is always a circle.

2.3.1 Circular Cross-Section. A circular cylinder with the radius R gliding at a velocity G in the direction of the positive X axis can be replaced with a dipole of the strength

$$D = GR^2 . \tag{1}$$

The dipole is oriented in the direction of the positive X axis. A dipole is the threshold case of a source and a sink with the strengths $+m$ and $-m$ when the distance a between them disappears as they approach zero but at the same time the variable $m \cdot a$ (strength of the dipole) still has a defined value.

2.3.2 Elliptical Cross-Section. One proceeds from a circle in the Z plane with its center at the zero point (broken line in Fig. 2). Such a circle can be transformed into an ellipse in the W plane with conformal mapping. The transformation is carried out according to:

$$W = Z + (C^2/Z), \tag{2}$$

where $W=u+iv$ and $Z=x+iy$ and C is a constant. The constant C in this equation is equal to half the distance between the zero point and a focal point of the ellipse in the Wplane. A gliding circular cylinder can be replaced by a dipole as shown above. If it were possible to transform this dipole substitute for a circular cylinder in the Z plane into the W plane, one would obtain the substitute configuration for a cylinder with an elliptical cross-section. This, however, is not directly possible due to the transformation properties from the above equation according to which the Z plane is mapped in two planes, the so-called Riemann planes. Anything outside a circle of the diameter $2C$ is mapped in one Riemann plane, termed the W plane here, and anything inside such a circle is mapped in another Riemann plane, W'. The two Riemann planes are connected by a so-called branch cut between the focal points of the ellipse, i.e., between $u=2C$ and $u=-2C$. This branch cut corresponds to the circle C with the diameter $2C$ in the Z plane.

The indirect way of transforming the dipole inside the circle C in the Z plane into the Wplane consists in transforming the current it causes at the circumference of the circle C instead of transforming the dipole itself. The current is resolved into its radial and tangential components. The radial components are then to be understood as line distributions of sources or sinks on the circle circumference, viz., as sources for positive (from inside to outside) components, and as sinks for negative (from outside to inside) ones. The tangential components are interpreted as line distributions of circulations on the circumference. According to the direction of rotation of the tangential components relative to the center point of the circle, the circulations are assigned a positive (clockwise) or negative (anticlockwise) sign. The source, sink and circulation line distributions on the circle circumference can then be transformed into the W plane at the branch cut between $2C$ and $-2C$. Each point on the branch cut corresponds to two points on the circle C in the Z plane, the positions of which are symmetrical relative to the x axis. This means that the line distribution of the branch cut is the sum of the line distributions on the circumference half symmetrical to the x axis.

Before the transformation of these line distributions from the Z into the Wplane, however, it must be taken into account that a permanent dipole belonging to circle C exists in the Z plane which must not be transformed into the W plane. This dipole has the strength

$$D_c=G\cdot C^2\,.$$

The dipole to be transformed has the strength

$$D=G\cdot R^2-G\cdot C^2\,, \tag{3}$$

where G is the gliding velocity of the cylinder, and R the radius of the circle in the Z plane corresponding to the ellipse in the W plane.

The complex potential function $F(Z)$ for the current field of the dipole is

$$F(Z)=-D/Z \tag{4}$$

from which the potential function $P(Z)$ is derived as the real component of $F(Z)$:

$$P(Z)=Re\{F(Z)\} \tag{5}$$

with $Z=r\cdot e^{i\theta}$ (representation of Z in polar coordinates). It follows that the radial current velocity components at the circumference of the circle C are

$$S_{rc}(\theta)=(dP/dr)c=D\cdot\cos(\theta)/C^2 \tag{6}$$

and the tangential components

$$S_{tc}(\theta)=(1/r)\,(dP/d\theta)c=D\cdot\sin(\theta)/C^2\,. \tag{7}$$

One can see from the equations for S_{rc} and S_{tc} that the radial components have the same amplitude and the same sign symmetrically to the x axis, while the tangential components have the same amplitude but different signs. On transformation into the Wplane, the current components on the circumference of the circle C are summated symmetrically to the x axis as already mentioned. This means that the line distributions of sources and sinks on the branch cut in the Wplane double their strength while the circulation line distributions cancel each other out.

The strength of the source or sink line distribution in a small differential sector of the circumference of the circle C is

$$dM_z(\theta)=S_{rc}(\theta)\cdot C\cdot d\theta\,. \tag{8}$$

In accordance with the conservation law of mass $dM_z(\theta)$ has to be transformed into the W plane as $dM_w(u)$ with the same strength. The following equation can be substituted for $dM_w(u)$:

$$dM_w(u)=S_{uc}(u)du\,, \tag{9}$$

where $S_{uc}(u)$ is the line distribution density of sources and sinks on the branch cut. The solution of this equation for $S_{uc}(u)$ is

$$S_{uc}(u)=(D\cdot u/C^2)/(4C^2-u^2)^{1/2}\,. \tag{10}$$

The substitute configuration for a cylinder with elliptical cross-section is then the source and sink line distribution on the line between the two focal points of the ellipse with the line distribution density $S_{uc}(u)$.

2.3.3 Fish-Shaped Cross-Section. If, in the Z plane, the concentric circle R is shifted to the right until it touches the circle C at the point $-C$ (solid line circle in Fig. 2),

then a figure in the W plane resembling the fish-shape corresponds to the shifted circle. This figure is called a symmetrical Joukowsky profile (Betz, 1964).

In this case, the dipole of the circle R in the Z plane is situated at

$$x = R - C = L \tag{11}$$

and has the strength

$$D_r = G \cdot R^2 .$$

Before transforming into the W plane, the radial components $S_{rc}(\theta)c$ of the permanent dipole must be subtracted from the radial components of this dipole $S_{rc}(\theta)r$ on the circle C. For the radial components to be transformed, one obtains the following expression:

$$\begin{aligned} S_{rc}(\theta) &= S_{rc}(\theta)r - S_{rc}(\theta)c \\ &= D_r((C^2+L^2)\cdot\cos(\theta) - 2LC)/ \\ &\quad (C^2+L^2-2LC\cdot\cos(\theta))^2 \\ &\quad - D_c\cdot\cos(\theta)/C^2 . \end{aligned} \tag{12}$$

After the transformation into the W plane, the resulting substitute configuration for the source and sink line distribution density for a cylinder with a fish-shaped cross-section is

$$\begin{aligned} S_{uc}(u) &= (((C^2+L^2)\cdot u - 4LC^2)/(C^2+L^2-Lu)^2) \\ &\quad \cdot D_r/(4C^2-u^2)^{1/2} \\ &\quad - D_c\cdot(u/C^2)/(4C^2-u^2)^{1/2} . \end{aligned} \tag{13}$$

To carry out the calculation, the continuous line distribution of the branch cut was converted into discrete sources and sinks. The number of discrete sources and sinks was limited to a total of 20 to avoid large calculation effort.

2.4 Reflection of the Substitute Configuration and Calculation of the Current Velocity

The calculation is carried out for the case in which the stationary cylinder has a circular cross-section.

2.4.1 The Gliding Circular Cylinder. Since the cross-section of the g. Cyl. is a circle here, the whole calculation will be carried out in the Z plane. As shown above, the substitute for a gliding circular cylinder is a dipole. To facilitate imaging the dipole, the coordinate System Z, at the zero point of which the center point of the g. Cyl. is situated, is transformed into a new coordinate system Z', at the zero point of which the center point of the s. Cyl. is situated, and on the horizontal axis of which the dipole is situated. The relation between Z and Z' is

$$Z' = Ze^{-ia} - |Zo| , \tag{14}$$

where $Zo = xo + iyo$ are the center point coordinates of the s. Cyl. in Z, and $a = \arctan(yo/xo)$.

The complex potential function for the current field of the dipole D_g in the coordinate system Z' is

$$F_g(Z') = -D_g\cdot e^{-ia}/(Z' + |Zo| - X_n) . \tag{5}$$

X_n is introduced to adapt the function F_g to the requirements of the iteration procedure which implements the interaction between the two cylinders. In the first iteration step X_n has the value zero, in subsequent steps, however, values greater than zero.

To obtain the complex potential function for the dipole imaged in the s. Cyl. F_h, Z' is replaced by R_0^2/Z' in the complex conjugated potential function F_g^* where R_0 is the radius of the s. Cyl.

$$\begin{aligned} F_h(Z') &= F_g^*\cdot(R_0^2/Z') \\ &= -D_g\cdot e^{ia}/((R_0^2/Z') + |Zo| - X_n) . \end{aligned} \tag{16}$$

Then, after retransformation to the Z coordinate

$$F_h(Z) = -D_h\cdot e^{i(\pi+a)}/(Z\cdot e^{-ia} - L_h) , \tag{17}$$

where

$$D_h = D_g\cdot R_0^2/(|Zo| - X_n)^2$$

and

$$L_h = |Zo| - R_0^2/(|Zo| - X_n) .$$

To image the substitute dipole of the s. Cyl. back into the g. Cyl., one proceeds as before. In the complex conjugated potential function F_h^*, Z is replaced by R^2/Z, where R is the radius of the g. Cyl. The equation for the re-imaged dipole F_{gh} is then

$$F_{gh}(Z) = -D_{gh}\cdot e^{-ia}/(Z\cdot e^{-ia} - L_{gh}) , \tag{18}$$

where

$$D_{gh} = D_h\cdot R^2/L_h^2$$

and

$$L_{gh} = R^2/L_h .$$

In the next iteration step, the dipole strength D_g is replaced by D_{gh} in the equation for F_g, and X_n is equated to the value of L_{gh}.

As can be seen from the equations for D_h and D_{gh}, the dipole strength is multiplied by the factor K

$$\begin{aligned} K &= R_0^2 R^2/((|Zo| - X_n)^2 \\ &\quad \cdot (|Zo| - R_0^2/(|Zo| - X_n))^2) \end{aligned} \tag{19}$$

at each iteration step. If the value for K is smaller than 1.0 then the convergence requirement for the iteration is met. For a certain value of R, the factor K tends to increase as R_0 increases. R_0 has its maximal value, viz., infinity, for a flat wall. In this case the maximal value

for X_n is

$$X_{n.\max} = R + b - (b^2 + 2bR)^{1/2}, \tag{20}$$

where b is the distance between the wall and the cylinder.

If one calculates the limit of K for $R_0 = \infty$, one obtains

$$\lim_{R_0=\infty} K = R^2/(R + b + (b^2 + 2bR)^{1/2})^2. \tag{21}$$

For values of $b > 0$, $\lim_{R_0=\infty} K < 1.0$.

This meets the convergence requirement for the iteration procedure as long as there is a space between the two cylinders.

The potential function for the current evoked by the presence of the s. Cyl. is the sum of the real components of the complex potential functions F_h and F_{gh}. The derivation of the potential function according to x or y respectively leads to the current velocities dC_{vx} or dC_{vy} respectively. The result for an iteration step is then

$$\begin{aligned} dC_{vx}(x, y)_n = D_{hn} \cdot (Y_{sh}^2 \cdot \cos(2a) - X_{ch}^2 \cdot \cos(2a) \\ - 2 \cdot X_{ch} \cdot Y_{sh} \cdot \sin(2a))/M_h \\ - D_{ghn} \cdot (Y_{sg}^2 - X_{cg}^2)/M_g \end{aligned} \tag{22}$$

and

$$\begin{aligned} dC_{vy}(x, y)_n = D_{hn} \cdot (X_c^2 \cdot \sin(2a) - Y_{sh}^2 \cdot \sin(2a) \\ - 2 \cdot X_{ch} \cdot Y_{sh} \cdot \cos(2a))/M_h \\ - D_{ghn} \cdot (2 \cdot X_{cg} \cdot Y_{sg})/M_g \end{aligned} \tag{23}$$

where

$$M_h = (X_{ch}^2 + Y_{sh}^2)^2,$$

$$M_g = (X_{cg}^2 + Y_{sg}^2)^2,$$

$$X_{ch} = x - L_{hn} \cdot \cos(a),$$

$$Y_{sh} = y - L_{hn} \sin(a),$$

$$X_{cg} = x - L_{ghn} \cos(a)$$

and

$$Y_{sg} = y - L_{ghn} \sin(a).$$

If these components are added for the iteration steps which follow each other, the result is

$$dC_{vx}(x, y) = \sum_n dC_{vx}(x, y)_n$$

$$dC_{vy}(x, y) = \sum_n dC_{vy}(x, y)_n$$

and

$$dC_v(x, y) = (dC_{vx}(x, y)^2 + dC_{vy}(x, y)^2)^{1/2}. \tag{24}$$

Since the calculation was carried out numerically on a computer, the iteration was interrupted as soon as the additional values for dC_v became smaller than 10^{-3} of their value in the first iteration step.

2.4.2 The Gliding Cylinder with an Elliptical Cross-Section. As shown above, the gliding elliptical cylinder can be replaced by a configuration of discrete sources and sinks. In the coordinate system $W = u + iv$, each source or sink has the coordinates W_q, and the center point of the s. Cyl. has the coordinates W_h. To derive the function for the source imaged in the s. Cyl., the coordinate system W is transformed into the coordinate system W' according to the relation $W' = W - W_h$. The complex potential function F_g for the current field of the source with the strength is then

$$F_g(W') = Q \cdot \ln(W' - W_q'). \tag{25}$$

By replacing W' with R_0^2/W', where R_0 is the radius of the s. Cyl., in the complex conjugated function F_g^*, one obtains the complex potential function for the imaged source F_h

$$F_g^* \cdot (R_0^2/W') = Q \cdot \ln(R_0^2/W' - W_q'^*) = F_h(W'). \tag{26}$$

After retransformation to the W coordinate, the function F_h is

$$\begin{aligned} F_h(W) = Q \cdot (\ln(W_h - W_q) - \ln(W - W_h) \\ + \ln(W - (W_h + R_0^2/(W_q - W_h)^*))). \end{aligned} \tag{27}$$

The first term $(\ln(W_h - W_q))$ is a constant which contributes no value to the current velocity. The second term depends entirely on the coordinates of the s. Cyl. However, since each source Q has a corresponding sink $-Q$ in the substitute configuration, this term disappears through the summation of the functions of all sources and sinks in the configuration. The function $F_h(W)$ then becomes

$$F_h(W) = Q \cdot \ln(W - (W_h + R_0^2/(W_q - W_h)^*)). \tag{28}$$

According to the function F_h, the imaged source has the strength Q and the coordinates $W_{qh} = W_h + R_0^2/(W_q - W_h)^*$.

For imaging in the g. Cyl. the imaged source must first be transformed to the Z plane with the aid of conformal mapping. In the Z plane the ellipse appears as a circle. In the Z plane the complex potential function is then

$$F_h(Z) = Q \cdot \ln(Z - Z_{qh}).$$

After imaging in the g. Cyl. one obtains

$$F_{gh}(Z) = Q \cdot \ln(Z - R^2/Z_{qh}^*)$$

for the re-imaged source. The sum of the real components is the result of the potential equation for the

current change in the field for one iteration step. For further iteration steps, the re-imaged source has to be transformed to the W plane and imaged in the s. Cyl.

The derivation of the potential equation according to x or y respectively results in the current velocities dC_{vx} or dC_{vy} respectively. For an iteration step n and a source or a sink m, the result is then

$$dC_{vx}(x,y)n,m = Q_m \cdot ((x - X_{qh,nm})/D1 + (x - R^2 \cdot X_{qh,nm}/|Z_{qh,nm}|^2)/D2), \quad (29)$$

$$dC_{vy}(x,y)n,m = Q_m \cdot ((y - Y_{qh,nm})/D1 + (y - R^2 \cdot Y_{qh,nm}/|Z_{qh,nm}|^2)/D2), \quad (30)$$

where

$$D1 = (x - X_{qh,nm})^2 + (y - Y_{qh,nm})^2,$$

$$D2 = (x - R^2 \cdot X_{qh,nm}/|Z_{qh,nm}|^2)^2 + (y - R^2 \cdot Y_{qh,nm}/|Z_{qh,nm}|^2)^2$$

and

$$|Z_{qh,nm}|^2 = X_{qh,nm}^2 + Y_{qh,nm}^2.$$

The total change then results after forming the sum over n and m as

$$dC_v(x,y) = \left(\left(\sum_{n,m} dC_{vx}(x,y)_{n,m}\right)^2 + \left(\sum_{n,m} dC_{vy}(x,y)_{n,m}\right)^2\right)^{1/2}. \quad (31)$$

By inserting the coordinates x and y of the transformed contour points of the ellipse into the Z plane one obtains the values for the velocity change at this point in the Z plane. To obtain the corresponding values in the W plane, $dC_v(x,y)$ must be multiplied with a transformation factor Tf,

$$Tf = (((1 - C^2(x^2 - y^2)/Z^4)^2 + (2C^2xy/Z^4)^2)^{1/2})^{-1}. \quad (32)$$

The iteration was discontinued as soon as the additional values for dC_v became smaller than 10^{-3} of their value in the first step.

2.4.3 The Gliding Cylinder with Fish-Shaped Cross-Section. There is no essential difference between the calculation of the velocity change in this case and in that of the elliptical cylinder. As mentioned above, the fish shape in the W plane corresponds to a circle shifted to the right in the Z plane so one must only take into account the new coordinates of this circle in the calculation. There is, however, one difference from the ellipse, namely that the profile point in the W plane corresponds to a singular point $x = -C$ in the Z plane. This means that the current velocity must have the value zero at this point. Consequently, a circulation appears which makes the current velocity at the profile point equal to zero. The additional amount of this circulation must then be added to the current velocity.

3 Results

To facilitate understanding, the gliding cylinder will be designated according to its cross-section shapes, i.e., circle, ellipse and fish, while the term "obstacle" will be used for the stationary circular cylinder in the following. The calculation was performed for the following measurements of the three shapes in arbitrary units:

Circle: diameter 40 units.

Ellipse: width 40 units, length 100 units.

Fish: width 40 units, length 100 units.

The diameter of the obstacle was 40 units. The "parallel interval", defined as the distance between the surface of the obstacle and the surface of the gliding cylinder when its widest section was opposite the obstacle, was 1 unit.

The widths of the three shapes vertical to the gliding direction were made equal so as to be able to equate the amount of water displaced per time unit in the three cases at the same gliding velocity G.

3.1 Current Velocity Distribution (CVD)

The distribution of the current velocity C_v along the extended contour line of the circle, ellipse and fish respectively gliding past the obstacle is shown in Fig. 3a, b and c respectively. Since the gliding velocity appears as a coefficient in the calculation, the values of C_v are represented as normed for G.

For the ellipse and the fish in Fig. 3b and c, L corresponds to the extended contour line of the circle belonging to each in the Z plane. Points on the line L are connected by lines to the corresponding points on the real contour line.

Each curve in these figures plots the current velocity distribution (CVD) for a certain position of the gliding cylinder relative to the obstacle. The curves shown shifted for the positions following each other are to be understood as a series of current velocity changes within the time t. Positive values for C_v indicate a current velocity relative to the surface of the gliding cylinder in the opposite direction to the gliding movement.

The first curve A in each of the Fig. 3a, b, and c represents the CVD at the position A of the gliding cylinder relative to the obstacle as is shown in the upper figures. The influence of the obstacle on the current around the gliding cylinder is very small at this position. The CVD is the same as for gliding in open

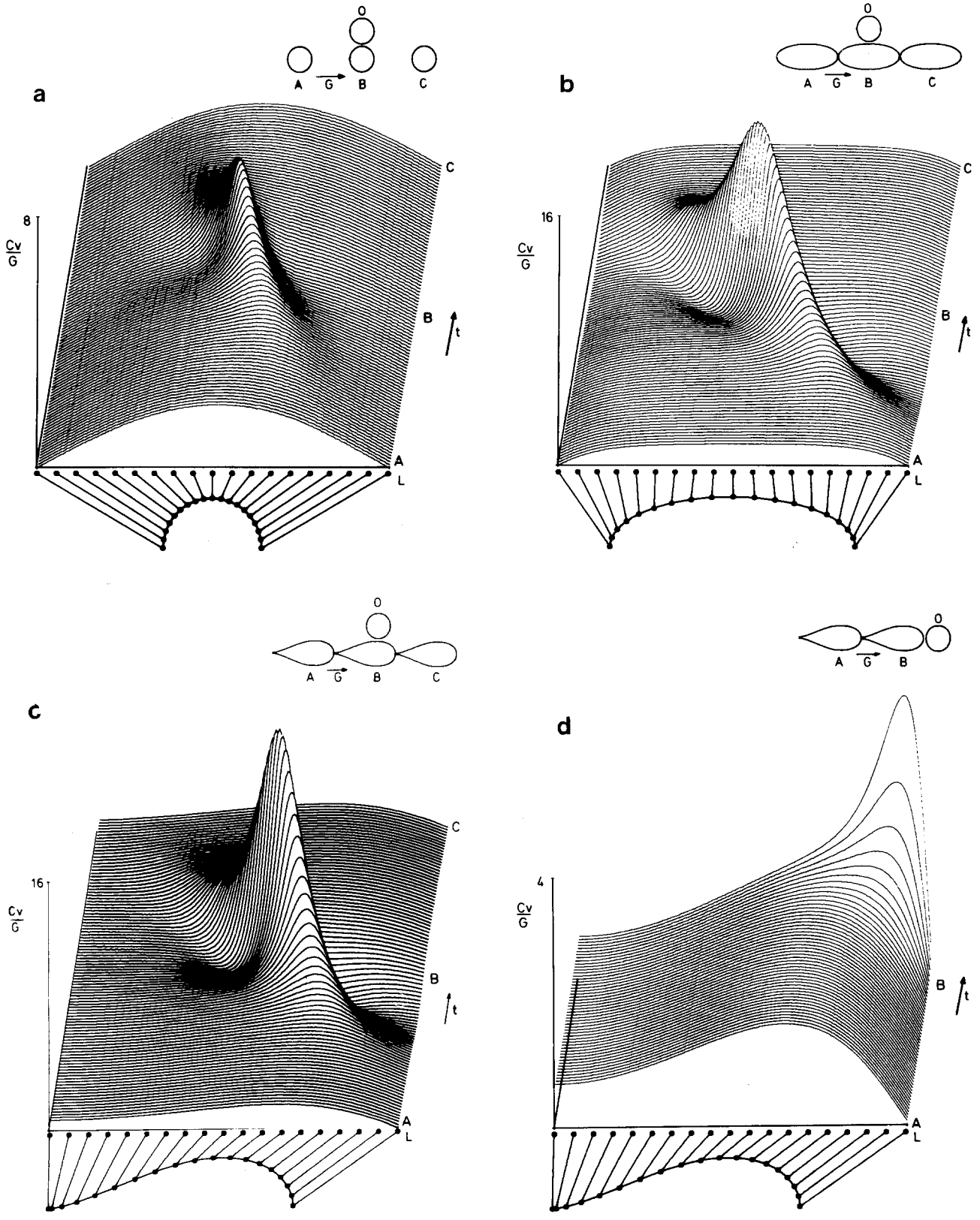

Fig. 3a–d. The current velocity distribution on the surface of a cylinder gliding past a stationary cylinder. **a** Gliding cylinder with a circular cross-section; **b** gliding cylinder with an elliptical cross-section; **c** gliding cylinder with a fish-like cross-section. **d** The current velocity distribution on the surface of a gliding cylinder with a fish-like cross-section approaching a stationary cylinder. G: gliding velocity; L: stretched contour of the g. Cyl.; t: time

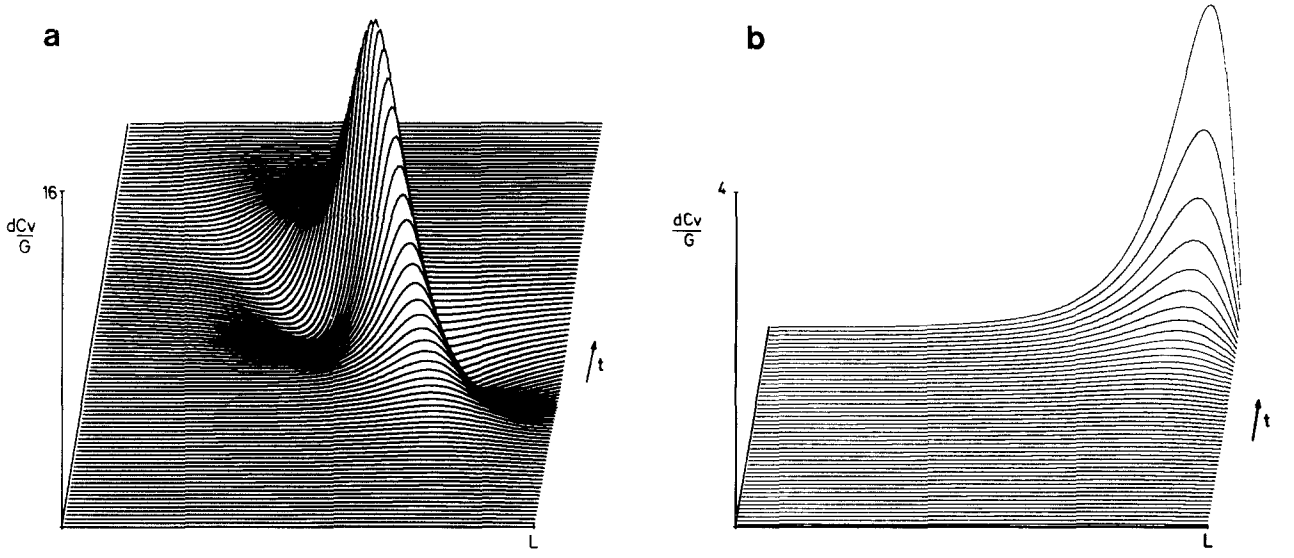

Fig. 4a and b. The change in the current velocity distribution (dC_v) on the surface of the gliding cylinder due to the stationary cylinder. **a** for the case of gliding past the stationary cylinder; **b** for the case of approaching the stationary cylinder

water. A wave forms in front of the gliding cylinder when this comes nearer to the obstacle. The wave reaches its maximum amplitude when the head of the gliding cylinder is opposite the obstacle (position *B*) and then dies away again at the tail end (position *C*).

Comparison of the three figures shows that the time and space course is similar for the three shapes. The maximum values for C_v, however, are different for the different shapes even though the amount of water displaced is the same in the three cases. The maximum value of C_v is lowest for the circle and highest for the fish. The explanation is that the proportion of displaced water which can flow around the outer sides of the obstacle and the circle (rather than between them) is higher than the proportion of displaced water which can flow around the outer sides of the obstacle and the fish.

The calculations were performed for the three shapes of the gliding cylinder so as to be able to compare the effect of the shape on the current generated. In the following, the fish shape alone will be considered.

The CVD was also calculated for the fish for the case where the gliding motion was directed frontally towards the obstacle (Fig. 3d). The first curve in Fig. 3d shows the CVD for the position *A* relative to the obstacle (cf. upper illustration). The influence of the obstacle on the current is once again very small. On further approach, C_v increases constantly at the head and then, in the last quarter of the distance, very strongly. The parallel interval at the last position *B* is 1 unit of the fish length.

So that the influence of the obstacle on the current around the gliding cylinder can be seen better, the current velocity change dC_v, which is obtained by subtracting the current velocity for gliding in open water C_{vo} from C_v, is shown for the cases of gliding past and frontal approach in Fig. 4a and b. These diagrams give an impression of the stimulus to the lateral line system according to the current field hypothesis mentioned in the introduction. To get an idea of the actual stimulus strength, the current changes shown in Fig. 4a and b should be taken as ratios of dC_v/C_{vo}.

Figure 5a and b show the value dC_v/C_{vo}, which indicates the degree of change in the current velocity for the same cases relative to that for gliding in open water. If the lateral line system functions according to the Weber-Fechner rule, this description will be the most appropriate. The large change at the head occurs because the values for C_{vo} in this area are very small. The absolute sensitivity of the sense cell will be the limit for the perception of stimulus details in the head region.

3.2 Pressure Distribution (PD)

After calculating the current velocity, the Bernoulli equation can be used to ascertain the pressure distribution and the pressure gradient on the surface of the gliding cylinder. The Bernoulli equation is:

$$(P-P_0)/(0.5\varrho C_{vo}^2)=1-((C_v^2)/(C_{vo}^2)).$$

Where P_0 and C_{vo} are the pressure and the current velocity in infinity, P and C_v the pressure and the current velocity at a certain point on the cylinder

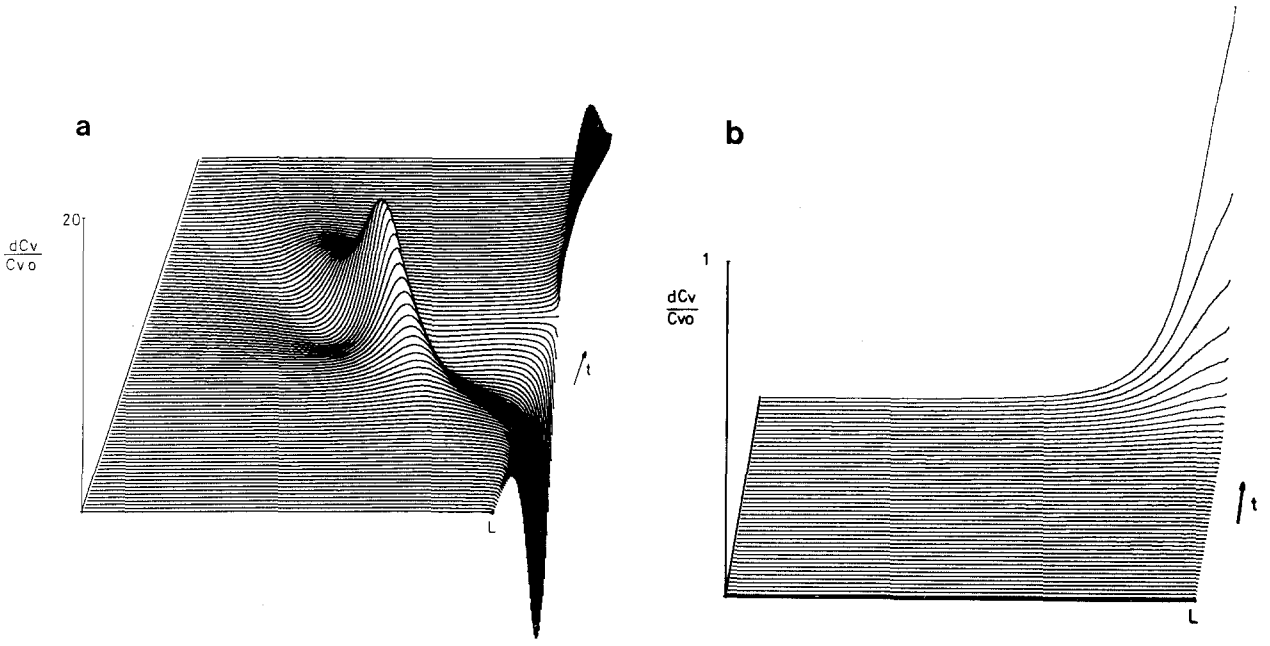

Fig. 5a and b. The degree of change in the current velocity distribution on the surface of the gliding cylinder due to the stationary cylinder. **a** for the case of gliding past the stationary cylinder; **b** for the case of approaching the stationary cylinder; dC_v: the change in current velocity; C_{vo}: the current velocity on the surface of the gliding cylinder in open water

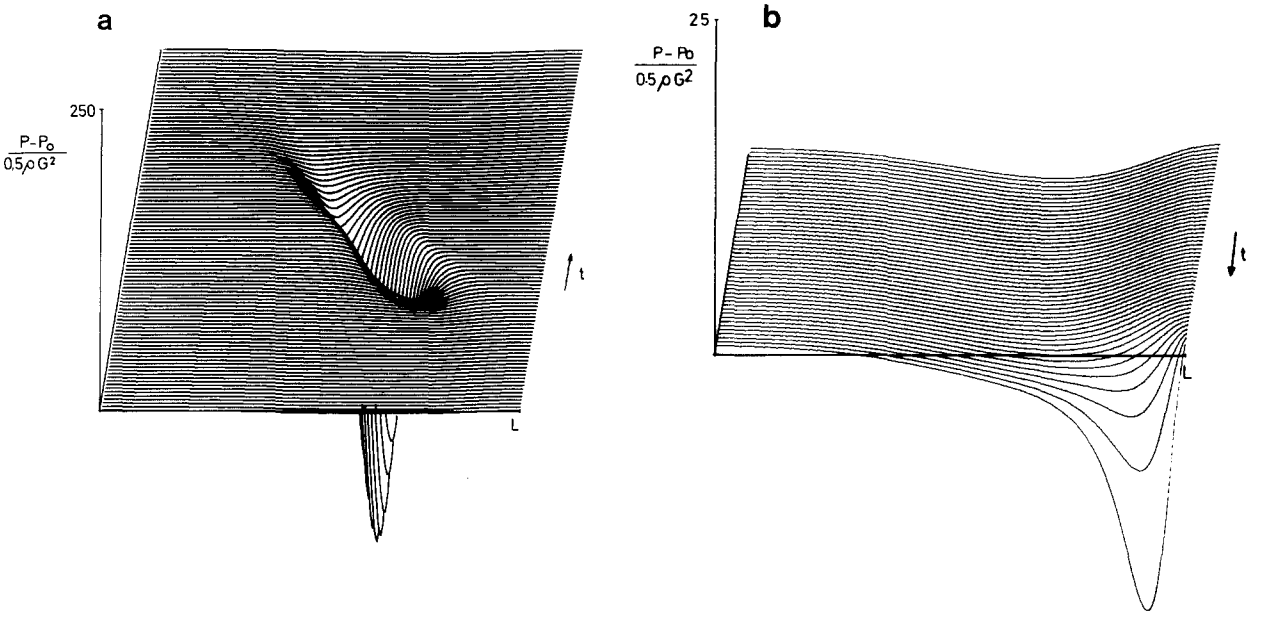

Fig. 6a and b. The pressure distribution on the surface of the gliding cylinder. **a** for the case of gliding past the stationary cylinder; **b** for the case of approaching the stationary cylinder

surface, and ϱ is the density of the water. A plot of this calculated pressure distribution is shown in Fig. 6a for the case of gliding past an obstacle, and in Fig. 6b for the case of frontal approach. The corresponding pressure gradients for the two cases are shown in Fig. 7a and b respectively.

3.3 Variations in Size and Distance of the Obstacle

In the gliding past case, the dependency of the current velocity distribution on the radius R_0 of the obstacle and on the parallel interval D were calculated (results

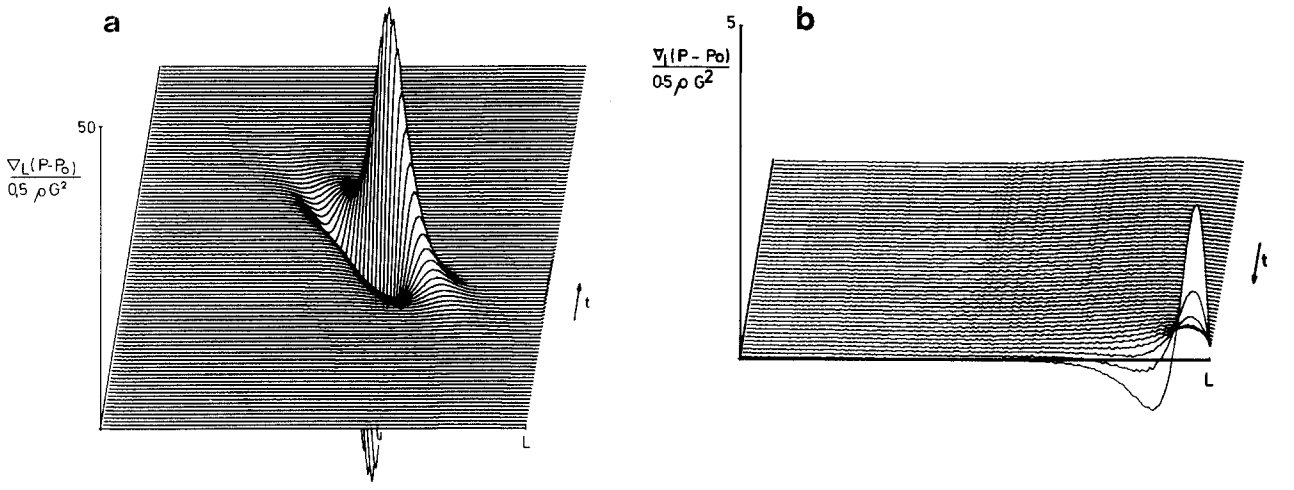

Fig. 7a and b. The pressure gradient on the surface of the gliding cylinder. **a** for the case of gliding past the stationary cylinder; **b** for the case of approaching the stationary cylinder

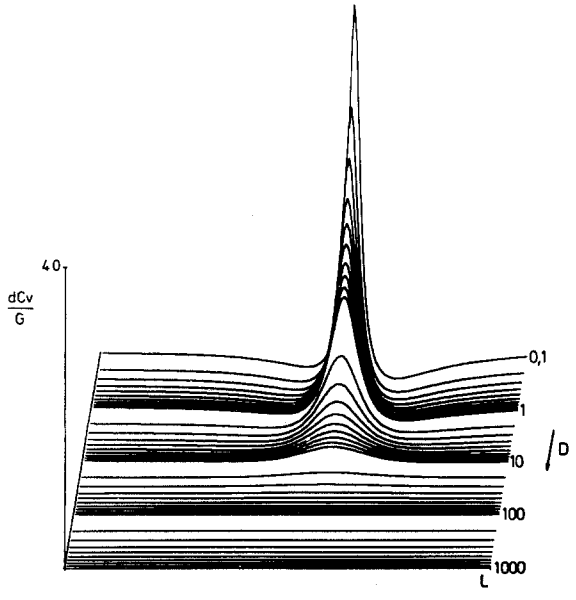

Fig. 8. Plot of the current velocity distribution as a function of the radius of the stationary cylinder R_0

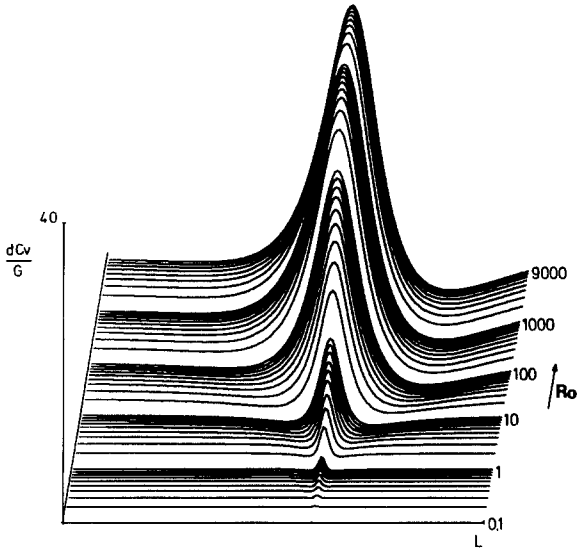

Fig. 9. Plot of the current velocity distribution as a function of the distance of the stationary cylinder from the gliding cylinder

shown in Figs. 8 and 9). The curves shown shifted are the spatial distribution of dC_v for a certain R_0 or D respectively at the moment when the gliding cylinder and the obstacle are on the same plane. The shift is made according to a logarithmic scale of the radius R_0 or the parallel interval D respectively.

To describe the influence of the size of the obstacle and its distance from the fish on the stimulus distribution two parameters for the current velocity distribution can be defined: the maximum positive amplitude $dC_{v.\max}$ and the width W. The width is defined as that length of the contour range in which dC_v has positive values. As can be seen from Fig. 8, $dC_{v.\max}$ and W increase as R_0 increases. When the parallel interval increases, $dC_{v.\max}$ is reduced while W is increased (cf. Fig. 9).

When the mode of representation is reversed, i.e., when $dC_{v.\max}$ and W are made the coordinate systems, and the corresponding combinations of the radius R_0 of the obstacle and the parallel interval D are plotted as points, and all points with the same value for the parallel interval are connected with a line, one obtains a group of curves such as is shown in Fig. 10. This means that there is an unequivocal combination of the size and the distance from the obstacle for every combination of $dC_{v.\max}$ and W.

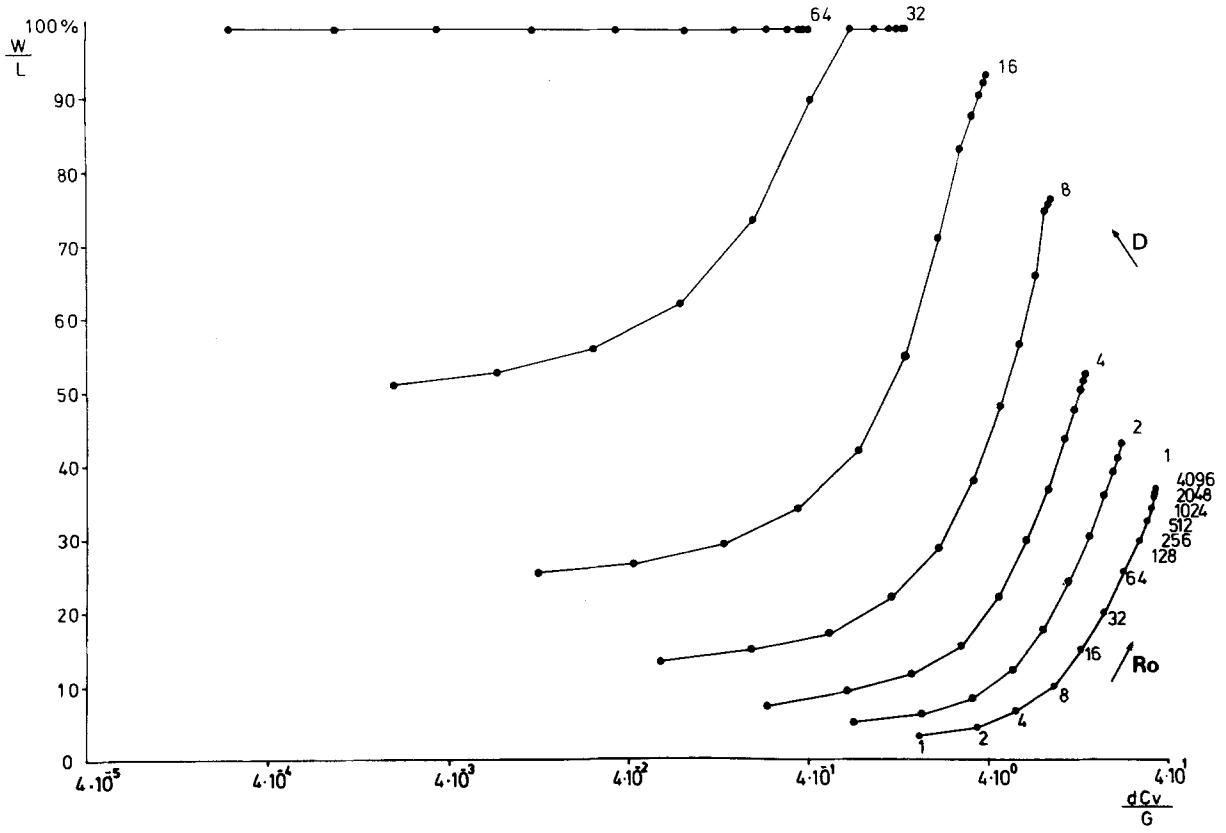

Fig. 10. Plot of the parameters of the stationary cylinder, its radius R_0 and its distance from the gliding cylinder D in a coordinate system established with the current velocity increase dC_v as the horizontal axis and the width W of the area in which the increase occurs expressed as a percentage of the contour length L as the vertical axis

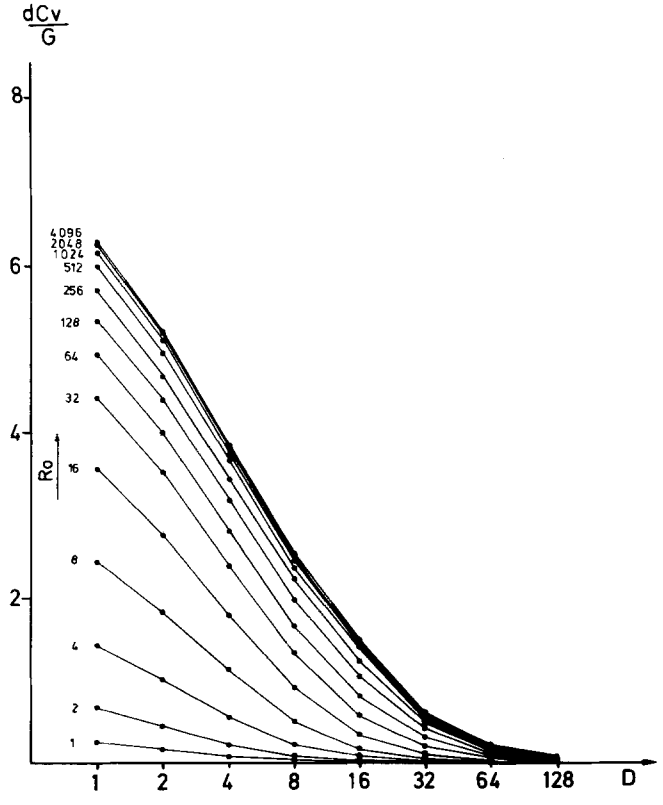

For the case of frontal approach, $dC_{v.\max}$ is shown in dependence on the distance between the fish's head and the surface of the obstacle for various radii of the obstacle in Fig. 11. As can be seen, one can define a range of up to 10 times the fish's length with respect to the radii of the obstacle in which $dC_{v.\max}$ increases. With respect to the parallel interval, it can be assumed that no noticeable increase in $dC_{v.\max}$ occurs until a distance shorter than the length of the fish is reached.

Discussion

This paper aims at describing the stimulus for the lateral line system mathematically, and in particular those stimuli which are the result of modifications to the current generated by the fish itself as it glides.

As the results show, a stationary obstacle in the vicinity of the gliding fish modifies the current field in such a way that a well defined spatial and temporal

Fig. 11. Plot of the current velocity increase in the case of approaching the stationary cylinder as a function of the distance D to it. The parameter for each curve is the radius of the stationary cylinder R_0

current velocity distribution (CVD) and a pressure distribution (PD) occur on the fish's body surface. It is of interest to note here that the gliding velocity of the fish enters into the calculation of the CVD as a coefficient. As a consequence, the spatial and the temporal distribution of current velocity and pressure will not be altered in their form when the gliding velocity varies; only the amplitude and time duration will be changed. This means that, for the fish to be able to analyse the stimuli on its body surface as well as to correlate the spatial and temporal distributions of the stimuli, the gliding velocity must be accessible to it as a scaling factor. In view of the dependency of boundary layer thickness and frequency content of the stimulus on the gliding velocity, there must be an optimal gliding velocity for the fish.

As described above, the CVD in the case of gliding past an obstacle (Fig. 3c) can be characterized by a limited area of increased current velocity with adjoining areas of reduced current velocity (CV). The width of these areas and the amplitude of the CV depend on the size of the obstacle and on its distance from the fish. The way in which these two parameters affect the CVD differs. For instance, an increase in the size of the obstacle yields an increase in the amplitude of the CV and in the width of the area in which this occurs (Fig. 8). By contrast, an increase in the distance of the obstacle from the fish leads to a smaller increase in the amplitude of the CV, while the width of the area of its occurrence increases (Fig. 9). These different tendencies of the chosen characteristics for the CVD, the amplitude of the increased CV and the width of the area in which it occurs, indicate the possibility that they could be used to code the size and distance of the obstacle. This possibility becomes clearer when all combinations of size and distance of the obstacle are plotted in a coordinate system in which the axes are the amplitude of the increased CV, and the width of its area. In such a representation, as Fig. 10 shows, different combinations of size and distance of the obstacle correspond to different points in the coordinate system. Consequently, the two value pairs can be transformed into each other. For the fish, this means that information can be gained on both the size and the distance of objects in its surroundings by analyzing the CVD on its whole body surface. In other words, a fish may not need a mechanism for size constancy.

It may be noted here that the accuracy with which a fish can analyse the CVD on its body surface depends on the number of CV measuring points on the surface, i.e., on the number of neuromasts. This may explain why a large number of neuromasts are found in certain species of fish such as the blind cave fish (Schemmel, 1967) which is thought to explore its surroundings by using the lateral line system.

In the case of frontal approach, the results showed that the CV does not increase noticeably until the fish is at a relatively short distance from the obstacle, and the increase occurs only in a limited area at the front region (Fig. 3d). In three-dimensional space, it is to be expected that increases in CV will be smaller since there is more space for the current to be deflected. Accordingly, one must conclude that a fish should be able to register very small changes in the CV in the region of its head, if it is to avoid an obstacle at a safe distance. The head is an area favorable for registering such small changes since the boundary layer on its surface is thinner than elsewhere on the body surface (Schlichting, 1951). It is possibly due to this demand on the lateral line system that the neuromasts are more numerous and the canal system has several organs in the head region.

The situation studied here is that of a fish gliding past or approaching a stationary obstacle. The contrary situation, that of a stationary fish and a moving object leads to a different CVD on the body surface of the fish. So, a fish in this situation experiences a different stimulus distribution from that generated when it glides itself. An interesting question arises in this connection: which parameters of the stimulus distribution does a fish use to recognize an object as having the same shape, even though the stimulus distribution arising on its body surface due to the object varies?

Acknowledgements. I wish to thank Prof. v. Campenhausen for critical reading of the manuscript. Valuable discussions with Prof. G. Schubert are gratefully acknowledged. Further I wish to thank Neil Beckhaus for translating the manuscript, as well as Ms. M. Grosz and Mr. W. Hoch for their help with the preparation of the manuscript.

Financial support by the Deutsche Forschungsgemeinschaft (Ca 34/4) is gratefully acknowledged.

References

Betz, A.: Konforme Abbildung. 2nd edn. Berlin, Heidelberg, New York: Springer 1964

Campenhausen, C. von, Riess, I., Weissert, R.: Detection of stationary objects by the blind cave fish *Anoptichthys jordani* (Characidae). J. Comp. Physiol. **143**, 369–374 (1981)

Curle, N., Davies, H.J.: Modern fluid dynamics, Vol. I. Incompressible flow. London: Van Nostrand 1968

Dijkgraaf, S.: Untersuchungen über die Funktion der Seitenorgane an Fischen. Z. Vergl. Physiol. **20**, 162–214 (1934)

Dijkgraaf, S.: Bau und Funktion der Seitenorgane und des Ohrlabyrinths bei Fischen. Exper. **8**, 205–244 (1952)

Dijkgraff, S.: The functioning and significance of the lateral line organs. Biol. Rev. **38**, 51–105, (1962)

Dijkgraaf, S.: Biological significance of the lateral line organs. In: Cahn, P. (ed.) Lateral line detectors, pp. 83–95. Bloomington, London: Indiana University Press 1967

Flock, A., Wersäll, J.: A study of the orientation of the sensory hairs of cells in the lateral line organ of fish, with special reference to the function of the receptors. J. Cell Biol. **15**, 19–27 (1962)

Görner, P.: Untersuchungen zur Morphologie und Elektrophysiologie des Seitenlinienorgans vom Krallenfrosch (*Xenopus laevis* Daudin). Z. Vergl. Physiol. **47**, 316–338 (1963)

Kuiper, J.W.: Frequency characteristics and functional significance of the lateral line organ. In: Cahn, P. (ed.): Lateral line detectors. pp. 105–121. Bloomington, London: Indiana University Press 1967

Schemmel, C.: Vergleichende Untersuchungen an den Hautsinnesorganen ober- und unterirdisch lebender Astyanax-Formen. Z. Morphol. Oekol. Tiere **61**, 255–316 (1967)

Schlichting, H.: Grenzschicht-Theorie. Karlsruhe: G. Braun 1951

Webb, P.W.: Fast-start performance and body form in seven species of teleost fish. J. Exp. Biol. **74**, 211–226 (1978)

Webb, P.W.: Der Fischkörper: Form und Bewegung. Spekt. Wissenschaft **9**, 84–97 (1984)

Weissert, R., Campenhausen, C. von: Discrimination between stationary objects by the blind cave fish *Anoptichthys jordani* (Characidae). J. Comp. Physiol. **143**, 375–381 (1981)

Received: January 10, 1985

Dr. El-S. Hassan
Arbeitsgruppe III (Biophysik)
Institut für Zoologie
Johannes-Gutenberg-Universität
Saarstrasse 21
D-6500 Mainz
Federal Republic of Germany